

Selective protected state preparation of coupled dissipative quantum emitters

D. Plankensteiner¹, L. Ostermann¹, H. Ritsch¹, and C. Genes^{1,*}

¹Institut für Theoretische Physik, Universität Innsbruck, Technikerstrasse 21a, A-6020 Innsbruck, Austria

*claudiu.genes@uibk.ac.at

ABSTRACT

Inherent binary or collective interactions in ensembles of quantum emitters induce a spread in the energy and lifetime of their eigenstates. While this typically causes fast decay and dephasing, in many cases certain special entangled collective states with minimal decay can be found, which possess ideal properties for spectroscopy, precision measurements or information storage. We show that for a specific choice of laser frequency, power and geometry or a suitable configuration of control fields one can efficiently prepare these states. We demonstrate this by studying preparation schemes for strongly subradiant entangled states of a chain of dipole-dipole coupled emitters. The prepared state fidelity and its entanglement depth is further improved via spatial excitation phase engineering or tailored magnetic fields.

Introduction

Ensembles of effective two-level quantum emitters consisting of single atoms, ions, or defects in solids are employed ubiquitously in quantum optics and quantum information.¹ They are the basis for precision spectroscopy or atomic clock setups, as well as for experiments testing fundamental concepts of quantum physics or implementations of the strong coupling cavity QED (quantum electrodynamics) regime.^{2,3} In the absence of direct particle-particle interactions, larger ensembles allow for faster, more precise measurements⁴ via a scaling of the effective single photon to matter coupling strength g by a factor \sqrt{N} (with system size N) and a reduction of the quantum projection noise (by $1/\sqrt{N}$).^{5,6}

For any precise measurement one has to externally prepare, control and measure the particle dynamics. Hence, the emitters are almost unavoidably coupled to their environment. A suitable theoretical framework to model such experiments is open system dynamics with a coupling to a fluctuating thermal bath. At optical frequencies this can often be approximated by the zero effective temperature electromagnetic vacuum field.^{7,8} Still, extra perturbations by a thermal environment and background gas collisions cannot be avoided.

In a laboratory experiment the particles need to be confined in a finite spatial volume that can be addressed by laser beams. Thus, increasing particle numbers will lead to higher densities, where direct particle-particle interactions as well as environmentally induced collective decoherence can no longer be neglected. For optical transition frequencies a critical density is conventionally assumed at the point where the average particle separation is of the order of an optical wavelength.⁹ Above this limit vacuum fluctuations tend to become uncorrelated and decay becomes independent. However, recent calculations have shown that collective states can exhibit superradiance and subradiance even at much larger distances¹⁰ as long as the bandwidth of the emission is small enough.

In many typical configurations and in optical lattices in particular, the particle-particle interaction is dominated by binary dipole-dipole couplings, with its real part inducing energy shifts and its imaginary part being responsible for collective decay.^{11,12} Generally, this interaction is associated with dephasing and decay. However, recently it has been found that under special conditions also the opposite can be the case and these interactions can lead to a synchronization¹³ or even a blockade of the decay.¹⁴

Oftentimes it is assumed that while such states exist, they cannot be prepared by lasers as they are strongly decoupled from the radiation fields. However, it was recently proposed that individual instead of overall addressing of the atoms can push the many particle system to evolve towards subspaces protected from decay or dephasing.¹⁵ When applied to Ramsey spectroscopy such states have been shown to exhibit frequency sensitivities superior even to those obtained from non-interacting ensembles.¹⁶ However, apart from special cases with an optimal lattice size and excitation angle, it is not so obvious how to implement such precise a control.

In this work we highlight the surprising fact that interaction induced level shifts can be used to aid in preparing such states. In many cases the magnitude of the shifts a state experiences and its lifetime are tightly connected allowing one to identify and address interesting states via energy resolution. As a generic ensemble we particularize to a 1D regular chain of quantum

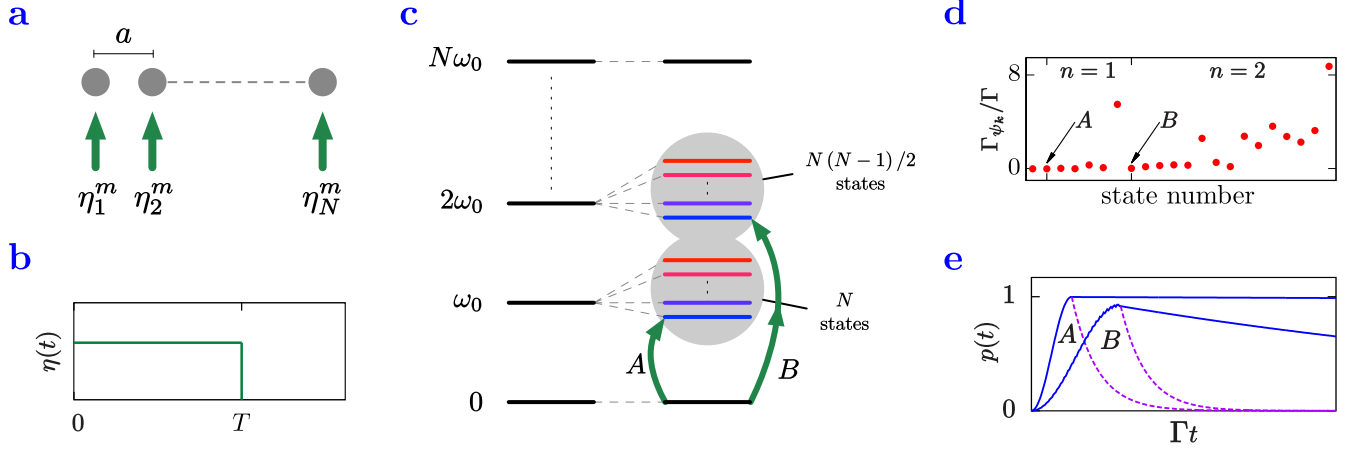


Figure 1. *Selective state preparation procedure.* **a)** A chain of N closely spaced quantum emitters (separation a with $ka \ll 1$, k being the laser wave number) are individually driven with a set of pumps $\{\eta_j^m\}$. **b)** The lasers are turned on for a time T , optimized such that an effective π -pulse into the desired subradiant target state is achieved. **c)** Level structure for the N systems where the C_n^N -fold degeneracy of a given n -excitation manifold is lifted by the dipole-dipole interactions. The target states are then reached by energy resolution (adjusting the laser frequency) and symmetry (choosing the proper m). **d)** Scaling of the decay rates of energetically ordered collective states starting from the ground state (state index 1) up to the single- and double-excitation manifolds for 6 particles at a distance of $a = 0.02 \lambda_0$. The arrows identify the decay rates for the lowest energy states in the single (A) and double (B) excitation manifolds. **e)** Numerical results of the time evolution of the target state population for $N = 6$ and $a = 0.02 \lambda_0$ during and after the excitation pulse. Near unity population is achieved for both example states A (where we used $\eta = 0.53 \Gamma$) and B (for $\eta = 2.44 \Gamma$) followed by a subradiant evolution after the pulse time T shown in contrast to the independent decay with a rate Γ (dashed line).

emitters coupled by dipole-dipole interactions with a tunable magnitude (by varying the interparticle separation). Collective coupling to the vacuum leads to the occurrence of subradiant as well as superradiant excitonic states.¹⁰ In particular, the subradiant states should prove extremely useful for quantum information as well as metrology applications as they exhibit robust, multipartite quantum correlations. As mentioned above, the atoms' interactions provide a first handle for target state selection as they lead to energy resolved collective states. Furthermore, using a narrow bandwidth laser excitation matched to the target states both in energy and symmetry allows for a selective population transfer from the ground state via an effective Rabi π -pulse.

In many cases, however, the required phase structure of the target state is not compatible with the excitation laser phase so that only a very weak coupling can be achieved. On the other hand, increasing the laser power reduces spectral selectivity by an unwanted addressing of off-resonant but strongly coupled states. Hence, to address a larger range of states of practical interest, we also propose and analytically study new methods of phase imprinting via a weak spatial magnetic field gradient. The small relative phase shifts increase the effective coupling to groups of emitters via a nonuniform phase distribution. With this method any state may acquire a finite laser coupling to the ground state via the magnetically induced level shifts resulting in an efficient population transfer with a minimal compromise on lifetime.

The considered setup is a chain (see Fig. 1a) of N identical two-level systems (TLS) with levels $|g\rangle$ and $|e\rangle$ separated by a frequency of ω_0 (transition wavelength λ_0) in a geometry defined by the position vectors $\{\mathbf{r}_i\}$ for $i = 1, \dots, N$. For each i , operations on the corresponding two-dimensional Hilbert space are written in terms of the Pauli matrices $\sigma_i^{x,y,z}$ and raising/lowering operators σ_i^\pm connected via $\sigma_i^x = \sigma_i^+ + \sigma_i^-$, $\sigma_i^y = -i(\sigma_i^+ - \sigma_i^-)$ and $\sigma_i^z = \sigma_i^+ \sigma_i^- - \sigma_i^- \sigma_i^+$. The complete Hamiltonian describing the coherent dynamics is

$$H = H_0 + H_{dip} = \omega_0 \sum_i \sigma_i^+ \sigma_i^- + \sum_{i \neq j} \Omega_{ij} \sigma_i^+ \sigma_j^-, \quad (1)$$

where H_0 is the free Hamiltonian and has degenerate energy levels (degeneracy $C_n^N = N!/(N-n)!n!$ for level n) ranging from 0 for the ground state to $N\omega_0$ for the highest excited state. The second term H_{dip} describes interactions between pairs of TLS which can be induced either by an engineered bath (such as a common, fast evolving optical cavity field) or by the inherent electromagnetic vacuum. We denote the couplings between emitters i and j by Ω_{ij} and particularize to the case of a free-space one dimensional equidistant chain of TLS with small interparticle distances a such that $a \ll \lambda_0$ (as depicted in Fig. 1a).

For the sake of simplicity, we use dipole moments perpendicular to the chain for all numerical computations. To a good

approximation, in the limit of $k_0 a \ll 1$, the nearest-neighbor (NN) assumption can be used (such that $\Omega_{ij} = \Omega \delta_{ij \pm 1}$) and exact solutions in the single-excitation manifold can be found.¹⁷ Within this subspace and approximation, the Hamiltonian assumes the form of a tridiagonal symmetric Toeplitz matrix with ω_0 on the diagonal and Ω above and below the diagonal. The solutions are readily available¹⁸ with eigenvalues $\omega_0 + \varepsilon_m$ for an index m running from 1 to N , where $\varepsilon_m = 2\Omega \cos[\pi m/(N+1)]$ are the dipole-induced energy shifts. The corresponding eigenstates of the Hamiltonian are then

$$|m\rangle = \sum_j f_j^m \sigma_j^+ |G\rangle, \text{ with } f_j^m = \sqrt{\frac{2}{N+1}} \sin\left(\frac{\pi m j}{N+1}\right), \quad (2)$$

where we used $|G\rangle = |g\rangle^{\otimes N}$.

Spontaneous decay via a coupling to the free radiation modes in the evolution of the system can be included in a generalized Lindblad form,⁸

$$\mathcal{L}[\rho] = \frac{1}{2} \sum_{i,j} \gamma_{ij} \left(2\sigma_i^- \rho \sigma_j^+ - \sigma_i^+ \sigma_j^- \rho - \rho \sigma_i^+ \sigma_j^- \right), \quad (3)$$

where the γ_{ij} denote collective damping rates arising from the coupling to a common radiation field. These rates also strongly depend on the atomic distances a with two prominent limiting cases of $\gamma_{ij}(a \rightarrow \infty) = \Gamma \delta_{ij}$ (independent emitters limit) and $\gamma_{ij}(a \rightarrow 0) = \Gamma$ (the Dicke limit¹⁹). In general, one can perform a transformation of the Liouvillian into a new basis by diagonalizing the γ_{ij} matrix. This procedure leads to a decomposition into N independent decay channels with both superradiant ($> \Gamma$) and subradiant (robust) decay rates ($< \Gamma$).¹⁶ Note, however, that the states corresponding to these channels generally do not coincide with energy eigenstates of the Hamiltonian, so that we cannot reduce the system dynamics to simple rate equations.

Results

Selective state preparation

Tailored coherent excitation. As mentioned above, our dipole coupled systems possess states with a large range of radiative lifetimes and energy shifts. Depending on the desired application particular states can be highly preferable over others. In a first straightforward approach we now illustrate that in principle it is possible to access a desired collective state simply by a selective coherent driving with a properly chosen amplitude and phase for each TLS. This is described by the Hamiltonian

$$H_m = \sum_j \eta_j^m (\sigma_j^+ e^{-i\omega_l t} + \sigma_j^- e^{i\omega_l t}), \quad (4)$$

with a suitably chosen set of η_j^m . For a targeted eigenstate in the single-excitation manifold, some analytical insight on how to choose these amplitudes can be gathered from the state's symmetry. For energy eigenstates this can be found quite reliably within the NN approximation.²⁰ In an equidistant finite chain our calculation suggests the following choice of driving fields at laser frequency ω_l ,

$$\eta_j^m = \eta \sin\left(\frac{\pi m j}{N+1}\right), \quad (5)$$

chosen to fit the symmetry of a target state $|m\rangle$.

The selectivity of the excitation process can be further improved by an *energetically resolved excitation* of a given state $|m\rangle$ by a proper choice of the laser frequency $\omega_l = \omega_0 + \varepsilon_m$ and its bandwidth. This is possible due to the interaction induced level splitting from H_{dip} (as depicted in Fig. 1c). Indeed, in perturbation theory and in a frame rotating at ω_l the evolution of the system starting from the ground state up to a normalization factor leads to

$$e^{-iH_m t} |G\rangle \simeq |G\rangle - i\eta t |m\rangle. \quad (6)$$

The success of the corresponding process is illustrated in the sequence of plots in Fig. 1, where the $|m=N\rangle$ state with $n=1$ is considered (target state A) and accessed via the combination η_j^N of pumps lasting for a duration T .

Numerical simulations were performed on a six-atom chain with driving strength $\eta = 0.53\Gamma$ at an interatomic separation of $a = 0.02\lambda_0$. The time for which the pumps are switched on is $T = 1.58\Gamma^{-1}$ which is considerably shorter than the time scale governed by the decay rate of 0.0009Γ of the target state. The resulting dynamic is an effective π -pulse (efficiency of 99.94%) flipping the population into the state $|m=N\rangle$ followed by an extremely slow decay, indicating the robustness of the target state (as seen in curve A of Fig. 1e).

It is, of course, desirable to target higher excitation manifolds as well. In the absence of analytical expressions or good approximations for the target states, we employ phases that yield maximal asymmetry, i.e. $\bar{\eta}_j = \eta(-1)^j$ for any $j = 1, \dots, N$. Such a driving can be expected to address collective states, where the fields emitted by any two neighboring particles interfere destructively¹⁴ (similar to a previously investigated mechanism¹⁵). Numerical simulations show that the resulting collective states indeed exhibit the lowest energy shifts of the targeted manifold and can be expected to be long lived. The resonance condition for a specific state $|\psi\rangle$ within the manifold n is $n\omega_l = n\omega_0 + \delta\omega_\psi$, where $\delta\omega_\psi = \langle\psi|H_{dip}|\psi\rangle$. As an illustration, the curve B in Fig. 1e shows an almost perfect efficiency (98.36%) two-photon π -pulse allowing for a population transfer to the longest-lived collective state in the second excitation manifold of $N = 6$ emitters separated by $a = 0.02\lambda_0$. The chain was driven with a strength of $\eta = 2.44\Gamma$ for a time $T = 3.44\Gamma^{-1}$, which again is significantly shorter than the natural time scale given by the target state decay rate of 0.0402Γ .

Let us add a comment on the practical implementation of such an addressing. In typical current experimental configurations for clocks based on 1D magic wavelength lattices^{21,22} the atoms are very close and hardly allow for an individual direct particle addressing. One is largely limited by a quasi plane wave driving, which typically addresses all particles with equal intensity. If the pump light is applied perpendicularly to the trap, the evolution is governed by a symmetric Hamiltonian H_{sym} , obtained from equation (4) with an equal pump amplitude $\eta_j^m = \eta$ for any m and j . A laser excitation from the ground state into the state $|m\rangle$ is connected to the coupling amplitude $\chi_m = \langle m|H_{sym}|G\rangle = \eta \sum_i f_i^m$, which yields

$$\chi_m = \begin{cases} 0 & \text{if } m \text{ is even,} \\ \frac{\sqrt{2}\eta}{\sqrt{N+1}} \cot\left(\frac{m\pi}{2N+2}\right) & \text{if } m \text{ is odd.} \end{cases} \quad (7)$$

We will refer to states with even m as *dark states* as they cannot be accessed by the laser excitation and call the remaining ones *bright states*.¹⁴ In the limit of large atom numbers $N \gg 1$, it is of interest to investigate the two cases, where $m \ll N$ and $m \sim N$, for states at the top/bottom of the manifold. In the first case, the function for the driving yields $\chi_m \approx \eta\sqrt{8N}/m\pi$, whereas in the other case we have $\chi_m \approx 0$.

Note, that sometimes geometry can change this behavior. For a 1D string of equidistant emitters illumination at a chosen angle of incidence and polarization leads to a designable phase gradient of the excitation amplitudes. The situation becomes even more complex for a 3D cubic lattice, where the phases also differ in the different lattice planes. As a lucky coincidence, a perpendicular plane illumination at the clock frequency in a magic lattice for Strontium (Sr) targets an almost dark state. This leads to subradiance and in principle allows for a spectral resolution better than the natural linewidth.²³ In not so favorable cases one could also think of a specific lattice design to facilitate a tailored dark state excitation.

Radiative properties. In order to be useful resources for quantum information applications, target states should exhibit *robustness* with respect to the environmental decoherence. To identify states of minimum decay rate, we scan through the eigenstates $|\psi_k\rangle$ of the Hamiltonian $H = H_0 + H_{dip}$ (for $k = 1, \dots, 2^N$) and compute their decay rates Γ_{ψ_k} (see section Methods below). We find that generally, for a given manifold, the energetic ranking of the states closely indicates their robustness to decay (as illustrated by the color-coding in Fig. 1c) ranging from blue for subradiant states to red for superradiant states. This is due to the fact that both radiation and energetic shifts are strongly dependent on the symmetry of the states. In Fig. 1d, for $N = 6$, we plot the decay rates of the collective states in the first ($n = 1$) and second ($n = 2$) excitation manifold arranged as a function of their increasing energy corresponding to the level structure of Fig. 1c. Superradiant states are found at the upper sides of the manifolds while the ideal robust states lie at the bottom. In Fig. 1d, the arrows indicate the optimal decay rates in the single- (0.0009Γ) and double-excitation manifolds (0.0402Γ) corresponding to target states A and B whose population evolution is depicted in Fig. 1e.

Within the single-excitation manifold, an analytical expression for the decay rate of a state $|m\rangle$ can be found as $\Gamma_m = \sum_{i,j} \gamma_{ij} f_i^m f_j^m$. For small distances the state $m = 1$ (upper state) is superradiant, whereas states at the bottom of the manifold $m \sim N$ exhibit subradiant properties. In the Dicke limit where $a = 0$ we have $\gamma_{ij} = \Gamma$ for any i and j , and we can compute $\Gamma_m = 2\Gamma \cot^2[m\pi/(2N+2)]/(N+1)$ for m odd and $\Gamma_m = 0$ for m even. Note, that in this particular limit, these are the same conditions as for the darkness and brightness of a state. For large numbers of emitters, we recover the expected superradiant scaling with N for the state with $m = 1$, i.e. $\Gamma_1 \approx 8\Gamma N/\pi^2$. On the other hand, large m yield a decay rate of $\Gamma_m \approx 0$ (perfect subradiance) in the same limit.

There are two important conclusions from these results: i) since in the considered limit the decay rate of the superradiant state $|m = 1\rangle$ scales with $\Gamma_1 \propto N$, whereas its driving is $\chi_1 \propto \sqrt{N}$, driving this state becomes more difficult with increasing atom number due to the reduced time-scale and ii) if the number of atoms is not too large, χ_m will remain finite, while Γ_m already indicates vast subradiance due to its scaling-down with N . Hence, there are robust states that remain bright, i.e. they can be driven directly even though the driving is not matched to their symmetry.

Accessing dark states via magnetic field gradients

The direct symmetric driving with H_{sym} allows access to bright states only. Given that nearby dark states can conceivably be more robust, we now employ a progressive level shifting mechanism that allows for a coupling between bright and dark states. This is achieved by subjecting the ensemble to a magnetic field with a positive spatial gradient along the chain's direction. The increasing energy shift of the upper atomic levels (as depicted in Fig. 2a) plays a role similar to the individual phase imprinting mechanism described previously. For each particle the shift of the excited level induces a time-dependent phase proportional to the value of the magnetic field at its position. We demonstrate the mechanism for a particular two-atom example, where indirect near unity access to the dark subradiant asymmetric collective state is proven and extend it to the single-excitation manifold of N atoms.

Two-atom case. The eigenstates of the Hamiltonian $H_0 + H_{dip}$ are $|E\rangle = |ee\rangle$, $|G\rangle = |gg\rangle$ and in the single-excitation subspace $|S\rangle = (|eg\rangle + |ge\rangle)/\sqrt{2}$ and $|A\rangle = (|eg\rangle - |ge\rangle)/\sqrt{2}$. The symmetric state $|S\rangle$ is superradiant ($\Gamma_S = \Gamma_1 = \Gamma + \gamma_{12}$) and bright, directly accessible via symmetric driving with strength $\chi_1 = \sqrt{2}\eta$. The asymmetric state $|A\rangle$, on the other hand, is subradiant ($\Gamma_A = \Gamma_2 = \Gamma - \gamma_{12}$) and dark. Indirect access can be achieved by shifting the second atom's excited state by $2\Delta_B$ (see schematics in Fig. 2b), where Δ_B is tunable and quantifies the per-emitter shift for a given magnetic field amplitude. We first analyze the dynamics in the absence of decay by solving the time-dependent Schrödinger equation governed by the Hamiltonian $H = H_0 + H_{dip} + H_{sym} + H_B$, where $H_B = 2\Delta_B\sigma_2^+\sigma_2^-$. We reduce the dynamics to three states, and assume a quasi-resonant Raman-like scheme where the population of $|E\rangle$ is at all times negligible. An effective two-level system arises (between the ground state and the asymmetric state; see section Methods below) and the resonance condition can be identified as

$$\Delta^{(2)} = -\Delta_B + \sqrt{\Delta_B^2 + \Omega^2 - 2\eta^2}, \quad (8)$$

with an effective Rabi frequency of

$$v_R^{(2)} = \frac{\sqrt{2}\eta\Delta_B}{\Omega + \sqrt{\Delta_B^2 + \Omega^2 - 2\eta^2}}. \quad (9)$$

To fulfill $|c_S|^2 \ll 1$, we need to restrict the driving to a parameter regime where $\eta, \Delta_B \ll \Omega$. A scan over the magnetic field is performed and the exact numerical results for the asymmetric state population are plotted in Fig. 2d against the adiabatic solution showing near unity population transfer for an optimized Δ_B . Further restrictions are imposed when decay is considered. These stem from the fact that the coherent process described by v_R should be faster than the incoherent one characterized by Γ_A . For close particles, the ability to tune the distance ensures that the scaling down of Γ_A is very fast and the above conditions are readily fulfilled. For the particular example illustrated in Fig. 2d we chose $a = 0.05\lambda_0$, resulting in $\Omega = 23.08\Gamma$, $\Gamma_A = 0.019\Gamma$. The 0.994 population is reached at $T = 16.19\Gamma^{-1}$, which is very close to the theoretical estimate of $T = \pi/2v_R^{(2)} = 16.179\Gamma^{-1}$ obtained from the adiabatic solution under the assumption of a π -pulse transferring the population to the target state.

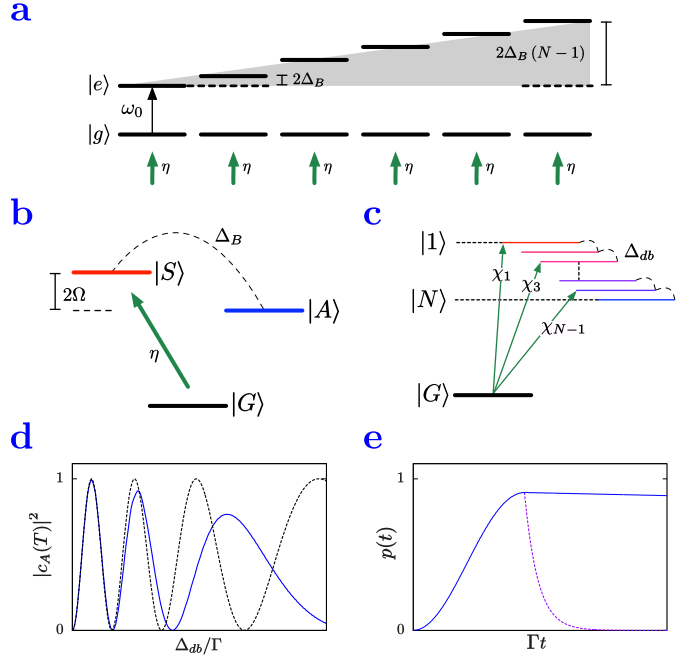


Figure 2. Coupling to dark states via a magnetic field gradient.

a) Linearly increasing level shifts along the chain occurring in the presence of the magnetic field gradient. **b)** Illustration of the level structure and indirect dark state access for two coupled emitters. While symmetry selects the state $|S\rangle$, off-resonant addressing combined with bright-dark state coupling of strength Δ_B allows for a near-unity population transfer into the state $|A\rangle$. **c)** Dynamics in the single-excitation manifold of N coupled emitters where symmetric driving reaches the bright states with amplitudes χ_m while the magnetic field couples neighboring dark and bright states. **d)** Plot of the asymmetric state population for the two-atom case as a function of the increasing magnetic field (solid line) compared to the steady-state approximation (dashed line) at numerically optimized time $T = 16.19\Gamma^{-1}$, with parameters $\eta = \Gamma$ and $a = 0.05\lambda_0$. **e)** For a chain of $N = 4$ emitters, a 91%-efficient π -pulse to the most robust state can be achieved as demonstrated in the population evolution plot. The separation is chosen to be $a = 0.025\lambda_0$, while $\eta = 40\Gamma$ and numerical optimization is employed to find $\Delta_B = 0.98\Gamma$.

Many-atom case. For a chain of N atoms, we consider the

progressive shifting of excited levels along the chain depicted in Fig. 2a. This is realized by the application of a magnetic field with a constant gradient and is described by the Hamiltonian $H_B = 2\Delta_B \sum_i (i-1) \sigma_i^+ \sigma_i^-$. Let us consider a dark state $|d\rangle$ (d even) and the bright state $|b = d-1\rangle$ immediately above. Their coupling via H_B is quantified by $\Delta_{db} = 2\Delta_B \sum_i (i-1) f_i^d f_i^b$, as shown in Fig. 2c.

We develop a protocol where direct off-resonant driving into the bright state (amplitude χ_b) combined with a coupling between the bright and dark states via the magnetic field leads to an almost unity population transfer into the dark state. Given a sufficient energy separation, the problem can be reduced to solving the time-dependent Schrödinger equation for the three coupled state amplitudes c_b, c_d and c_G . Following the same adiabatic approximation as in the two-atom case we reduce the general dynamics to an effective two-level system between the states meant to be connected by an effective π -pulse, i.e. $|d\rangle$ and $|G\rangle$. The generalized resonance condition (with $\varepsilon_{db} = \varepsilon_d - \varepsilon_b$) reads

$$\Delta^{(N)} = -\Delta_B(N-1) - \frac{\varepsilon_d + \varepsilon_b}{2} + \sqrt{\frac{\varepsilon_{db}^2}{4} + \Delta_{db}^2 - \chi_b^2}, \quad (10)$$

and was obtained in the limit where the coupling of the dark state to the other adjacent bright state $|d+1\rangle$ was neglected owing to the relation $\chi_{d-1} \gg \chi_{d+1}$. The effective transition rate between the ground state and the state $|d\rangle$ is

$$v_R^{(N)} = \frac{\chi_b |\Delta_{db}|}{\Delta + \varepsilon_b + \Delta_B(N-1)}. \quad (11)$$

The addition of decay imposes a new constraint on the timescale of the process, i.e. $v_R^{(N)} \gg \Gamma_d$, required to ensure near unity population in the dark state. The fulfillment of this condition depends on the individual system under consideration. As an illustration of the procedure, Fig. 2e presents the targeting of a robust dark state in the single excitation manifold of four particles. Note, that the numerical results are performed in an exact regime beyond the NN approximation and are in excellent agreement with our conclusions obtained from the NN treatment.

Discussions

Entanglement properties

To justify the usefulness of collective states for quantum information purposes, we employ the von Neumann entropy to analyze their entanglement properties. More specifically, we compute the von Neumann entropy of the reduced density matrix ρ_s of a single two-level emitter (showing the degree of its bipartite entanglement with the rest of the system) defined by $S(\rho_s) = -\sum_i \lambda_i \log_2 \lambda_i$, where λ_i is the i -th eigenvalue of ρ_s and $0 \log_2 0 \equiv 0$. We furthermore minimize the set of values for all atoms to obtain a lower bound on the entanglement contained in the system. We compare the numerical results to the single-atom entropy of the symmetric Dicke state $|-N/2, -N/2 + n\rangle$.¹⁹ For these particular states the entropy is maximized if the number of excitations in the state is $n = N/2$. It follows that it is highly desirable to drive the system into robust states as close as possible to $n = \lfloor N/2 \rfloor$ excitations (where $\lfloor N/2 \rfloor$ is the largest integer smaller or equal to $N/2$), since this manifold contains the most entangled state. A comparison of the exact numerical data and the analytical expression for the entropy is shown in Fig. 3a.

Another way to characterize the entanglement of the prepared state is to investigate their *depth of entanglement*,^{24,25} which does not quantify the entanglement itself but rather shows

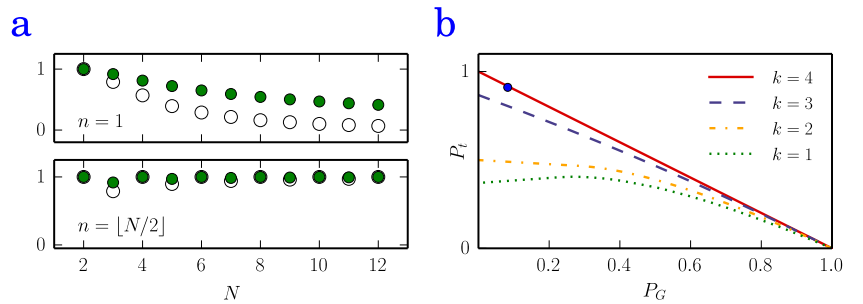


Figure 3. *Entanglement properties.* **a)** Comparison of the numerically computed von Neumann entropy (empty circles) of the reduced density matrix of the chain minimized over the atom index and the analytical expression for the entropy of the Dicke state (green circles), both for excitations $n = 1$ and $n = \lfloor N/2 \rfloor$ as a function of the atom number N at distance $a = 0.1\lambda_0$. **b)** Depth of entanglement of the subradiant four-atom state (blue dot) prepared by the magnetic field gradient scheme (see Fig. 2e). It clearly lies above the $k = 3$ boundary indicating four-atom entanglement. The k -atom entanglement boundaries of the target state population P_t as a function of the ground state population P_G have been computed for the corresponding target state of a four-atom chain at distance $a = 0.025\lambda_0$.

how many atoms of an ensemble are involved in the present entanglement.

This measure has been used in recent experiments^{25,26} since it is a readily measurable quantity. The depth of entanglement is computed as follows: given an N -atom target state in which an arbitrary number of said N atoms is entangled, we compute the limit of how much population one can drive into this state such that the resulting density matrix ρ remains separable into a subset of density matrices that exhibit no more than k -atom entanglement ($1 \leq k \leq N$). This may be done by numerically maximizing the target state population P_t as a function of the ground state population P_G for different k . The boundaries themselves indicate how many atoms need to be entangled in order to prepare the pure target state, i.e. the boundary where the target state population is maximized to 1 corresponds to the number of atoms entangled in the (pure) target state. If a general prepared state has a target and ground state population such that the corresponding data point lies on or above the k -atom boundary, more than k atoms are entangled.

Obviously, for the pure target states considered in the above computation all atoms contribute to the entanglement, since otherwise the minimal von Neumann entropy as shown in Fig. 3a would be zero. For a more interesting result, we can compute the depth of entanglement in order to demonstrate the efficiency of the driving procedure using a magnetic field gradient as in Fig. 2e. From Fig. 3b, where all boundaries have been plotted for the considered subradiant four-atom state, it is clear that the prepared state shows all-atom entanglement as the corresponding data point lies far above the boundary for three-atom entanglement.

Implementation considerations

The proof-of-principle technique presented above has been particularized on a specific generic system of emitters in an equidistant chain. The choice is natural since the electromagnetic vacuum provides a simple example for both collective dispersive and dissipative dynamics. To exemplify a possible realization we consider a particular system²⁷ where bosonic Sr atoms are trapped in a magic wavelength optical lattice at separations of $a = 206.4\text{nm}$. The working transition is at $\lambda_0 = 2.6\mu\text{m}$, between the 3P_0 and 3D_1 electronic states. This amounts to a ratio of $a/\lambda_0 \approx 1/13$ which allows for an operation in the regime targeted by our scheme. The corresponding single atom decay rate is at the order of $\Gamma = 0.3\text{ MHz}$ and circularly polarized light can allow for transitions between states with a difference of 1 in magnetic quantum number. We have numerically investigated a system of 4 atoms in such a configuration and found a sizeable 73% target state population for $\eta = 2\Gamma$ and $\Delta_B = 0.5\Gamma$, under the conditions of a relatively small level shift between the dark and bright state around 6Γ which does not allow for large driving powers. For further optimization of the efficiency of the target state preparation one could envision a modified setup where a trapping transition of smaller wavelength can be chosen that would most importantly allow for better state separation (owing to larger dipole shifts). The corresponding magnetic field gradient required to produce the considerable $\Delta_B = 0.5\Gamma$ shift on a distance of $a = 206\text{ nm}$ is around $5.2 \cdot 10^5\text{ G/m}$, not far from state-of-the-art values achievable in high magnetic field gradient magneto-optical trap experiments.^{28,29} Of course, there are many detrimental practical effects that can seriously limit the above technique such as light-assisted collision loss. We envision the extension of the described technique to systems where both the coherent and dissipative particle-particle interactions can be suitably tailored. For example, the same kind of dipole-dipole Hamiltonians can occur in 3D lattices of polar molecules³⁰ or between two different color NV centers in diamonds.³¹

Conclusions

Direct particle interactions are typically detrimental and limiting in precision measurement applications. Here, we have presented some specific opposite examples, where the *collective* nature of the decoherence combined with the coherent binary dipole-dipole interactions is used as a new resource for the controlled and efficient preparation of specially selected states. The excitation scheme can be tailored to address target states exhibiting both entanglement as well as robustness against decay. As a generic example we studied the case of a one-dimensional system of tightly spaced equidistant quantum emitters. Already the inherent dipole-dipole coupling allows for a targeted state preparation technique via energy selection. The performance of the excitation can be enhanced additionally via the *continuous* application of a spatially increasing magnetic field. The general principle of such a phase imprinting technique is potentially applicable in many specific environments such as optical lattices or atoms and ions localized within one or more common optical cavity modes,^{32,33} NV-centers or superconducting qubits coupled to CPW transmission lines or resonators.^{34,35}

Methods

Decay rate of the states

In order to arrive at an analytical expression for the decay rate of an eigenstate $|\psi_k\rangle$ of the Hamiltonian in equation (1), we consider the homogeneous part of the differential equation of the corresponding density matrix element that arises from the

master equation. The solution of this differential equation yields an exponential decay. The rate at which the state population decays may be written as

$$\Gamma_{\psi_k} = -\langle \psi_k | \mathcal{L} [| \psi_k \rangle \langle \psi_k |] | \psi_k \rangle = \sum_{i,j} \gamma_{ij} \langle \psi_k | \sigma_i^+ \sigma_j^- | \psi_k \rangle. \quad (12)$$

Note, that this is true only for states that contain one specific number of excitations, i.e. they are eigenstates of the operator $\sum_i \sigma_i^z$. Obviously, this is fulfilled for eigenstates of the considered Hamiltonian. Equation (12) was used in order to compute the rates depicted in Fig. 1d and throughout the manuscript. For example, we used it in order to compute the decay rate of the eigenstates in the NN approximation Γ_m .

Subradiance and disorder

Let us consider the influence of positioning disorder on subradiant properties of the target states. To mimic disorder we perturb an equidistant chain of N emitters (average separation a) by introducing an uncertainty in each emitter position quantified by a defect parameter s (normal distribution of variance sa). We then write the randomized matrix of decay rates and find the minimum decay channel without as well as in the presence of disorder of $s = 20\%$ and $s = 40\%$. For the $s = 0\%$ case, it has been shown¹⁶ that the minimum decay rate scales exponentially with N even for distances up to $0.4\lambda_0$, while the linear scaling with N typical for superradiance is reached for $a \ll \lambda_0$ only. After averaging over 100 random configurations, we plot the logarithm of the minimal rates as a function of increasing N in Fig. 4a.

As a somewhat surprising result, subradiance scales even better with N as the disorder increases. This might be understood as a destructive interference effect brought on by the cancelation of emitted photons stemming from the random positioning. As pointed out in previous investigations,¹⁶ the states of low symmetry (as, for example, the $m = N$ state) possess decay rates closest to the analytically derived minimal rate. We analyze the respective sensitivity of the state subradiance to disorder by initializing the system of N emitters in the $m = N$ state and allow it to decay. The outcome is plotted in Fig. 4b and shows remarkable robustness of the disordered systems on a long time-scale. While on a short time-scale disorder pushes the considered state into faster decaying channels, the long time limit shows that the remaining population accumulates in the disorder-enhanced robust states.

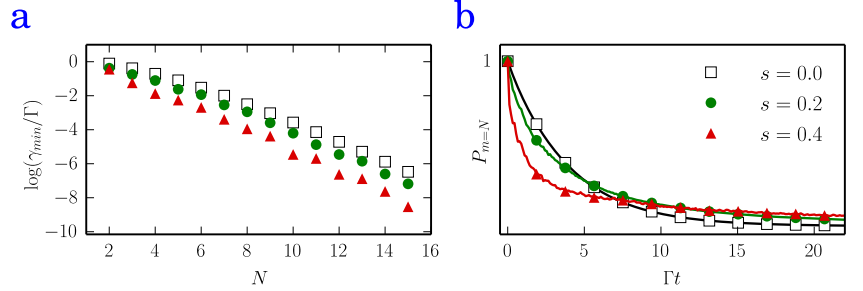


Figure 4. *Subradiance and disorder.* a) Plot of the logarithm of the minimal eigenvalue of the decay rate matrix (matrix with entries γ_{ij}) as a function of N at a distance of $a = 0.4\lambda_0$ for increasing levels of disorder ($s = 0, 0.2, 0.4$). b) Decay of the $|m = N\rangle$ state as a function of time. In the presence of disorder ($s = 0.2, 0.4$) the short time and long time behaviors are fundamentally different. At short times, disorder can push the state towards faster decaying channels while decay inhibition due to disorder occurs at larger times.

For short time-scales, the state still decays slowly (subradiantly), however, the decay rate increases with growing disorder ($s = 40\%$). More remarkable, though, is the behavior the decaying states show for long time-scales, as the states subject to larger disorder become more robust than the unperturbed system. This is due to the fact that all population in the $m = N$ state that decays through more radiative channels have decayed at that point and only the most subradiant channel (minimal eigenvalue of the decay rate matrix) remains. As seen in Fig. 4a, this eigenvalue is even further reduced by disorder which explains the long time-scale behavior in Fig. 4b.

Coherent dynamics with a magnetic field gradient

Two-atom case. To find the expressions in equation (8) and equation (9) we solve three coupled differential equations neglecting the population of the fully inverted state $|E\rangle$ as far off-resonant for all times. In the collective basis, where any state may then be written as $|\psi\rangle = c_S |S\rangle + c_A |A\rangle + c_G |G\rangle$, the equations are

$$i\dot{c}_S = (\Delta + \Delta_B + \Omega)c_S - \Delta_{BC}c_A + \sqrt{2}\eta c_G, \quad (13)$$

$$i\dot{c}_A = (\Delta + \Delta_B - \Omega)c_A - \Delta_{BC}c_S, \quad (14)$$

$$i\dot{c}_G = \eta c_S, \quad (15)$$

where $\Omega = \Omega_{12}$ is the coherent interaction between the atoms and Δ is the detuning between the atomic resonance frequency and the driving laser. For an efficient driving of $|A\rangle$ the population of the state $|S\rangle$ needs to be negligible which allows us to set a steady-state condition, namely $\dot{c}_S = 0$ yielding the desired effective two-level system between $|G\rangle$ and $|A\rangle$.

Many-atom case. The same approach as in the two-atom case may be used to describe the dynamics in the single-excitation manifold for an arbitrary number of atoms in a chain. Given sufficient energy separation we may neglect all states but the ones we aim to address. We can indirectly address a dark state $|d\rangle$ by driving the bright state $|b\rangle$ immediately above, which is coupled to the dark state by a magnetic field gradient. Neglecting all populations but c_b , c_d , and c_G and their respective couplings via the magnetic field gradient, the investigation reduces to the equations

$$i\dot{c}_b = [\Delta + \epsilon_b + \Delta_B(N-1)]c_b + \Delta_{db}c_d + \chi_b c_G, \quad (16)$$

$$i\dot{c}_d = [\Delta + \epsilon_d + \Delta_B(N-1)]c_d + \Delta_{db}c_b, \quad (17)$$

$$i\dot{c}_G = \chi_b c_b. \quad (18)$$

For an efficient driving of the dark state we may again invoke a steady-state condition on the bright state population $\dot{c}_b = 0$. This, again, yields an effective two-level system between the ground and the dark state with resonance condition and Rabi frequency as displayed in equation (10) and equation (11), respectively.

Von Neumann entropy

For a Dicke state an analytical expression for the von Neumann entropy of the reduced density matrix can be obtained. First, note that, since Dicke states are invariant under a permutation of the atoms, all reduced density matrices are identical. Hence, they all share the same von Neumann entropy for a given number of excitations n . We may choose to reduce the full density operator ρ to the density matrix of the first atom in the ensemble, i.e. $\rho_s^1 \equiv \rho_s = \text{tr}_{2,\dots,N}(\rho)$ which yields a von Neumann entropy of

$$S(\rho_s) = \frac{n}{N} \log_2 \left(\frac{N}{n} \right) - \left(1 - \frac{n}{N} \right) \log_2 \left(1 - \frac{n}{N} \right). \quad (19)$$

For the actual eigenstates of the Hamiltonian in equation (1) this computation needs to be done numerically. Furthermore, these states are not invariant under permutation of atoms and hence it is required to minimize the entropy with respect to the atomic chain index in order to find the lower bound.

Depth of entanglement

The boundaries depicted in Fig. 3b were found by maximizing the target state population with the condition on the density matrix of the prepared state to contain no more than k -atom entanglement, i.e. $\rho = \otimes_i \rho_i^{k_i}$ with $k_i \leq k$ and at least one $k_i = k$. To compute the boundaries we generalized the algorithm that was previously used solely for the W -state²⁵ to arbitrary states in the single-excitation manifold. For the computation of all boundaries we need to distinguish the two cases where $P_G = 0$ and $P_G > 0$. Considering a separable state ($k = 1$), the boundary for $P_G > 0$ is found to be

$$\max(P_t) = P_G \max_{\Pi_i \alpha_i = \sqrt{P_G}} \left| \sum_i |c_i| \frac{\sqrt{1 - \alpha_i^2}}{\alpha_i} \right|^2, \quad (20)$$

where $\alpha_i \in [0, 1]$ and c_i are the coefficients of the target state. For $P_G = 0$ the maximization is much simpler, i.e. $\max(P_t) = \max |c_i|^2$, which is found by setting one $\alpha_i = 0$ and the remaining coefficients $\alpha_{j \neq i} = 1$. Note, that for both these and all following computations we neglect the symmetry of the state, i.e. the phases of the coefficients c_i by using $|c_i|$. This is valid due to the invariance of entanglement under local unitary operations and necessary if we restrict the coefficients α_i in the way we did.

For multiple-atom entanglement ($k > 1$) the matter of finding the corresponding boundary is no longer so simple. In order to find the maximum population, we assume maximally allowed entanglement in the prepared state. We split the prepared state into $M = \lceil N/k \rceil$ sets, where $M-1$ sets are k -atom entangled and the remaining one is $k' = N - k(M-1)$ -atom entangled. To find the maximum, one has to consider all possible positions of the k' -entangled state. If, for example, the k' -entangled state is at the last position, the population of the target state $|t\rangle$ in the prepared state reads

$$P_t = \left| \langle t | \left[\left(\bigotimes_{i=1}^{M-1} |\varphi_i^k\rangle \right) \otimes |\varphi_M^{k'}\rangle \right] \right|^2, \quad (21)$$

where

$$|\varphi_i^k\rangle = \alpha_i |G_k\rangle + \sqrt{1 - \alpha_i^2} \sum_{r=1}^k \lambda_r^i \sigma_r^+ |G_k\rangle \quad (22)$$

is a general non-separable state of k atoms in the single-excitation manifold. The state $|G_k\rangle$ is the k -atom ground state and the coefficients $\lambda_r^i \in [0, 1]$ have to be normalized, i.e. $\sum_r (\lambda_r^i)^2 = 1 \forall i$. One then has to maximize the target state population with respect to the coefficients $\alpha_i \in [0, 1]$ and λ_r^i with the condition $\prod_j \alpha_j = \sqrt{P_G}$. The number of these coefficients, however, grows vastly with the number of atoms, hence numerical computations are limited. For $P_G = 0$ one can again choose one $\alpha_i = 0$ and all $\alpha_{j \neq i} = 1$.

Note, that all boundaries computed via this maximization only hold for pure states. In order to find the boundaries for mixed states we need to compute the convex hulls of the respective boundaries.²⁵ The $k = N$ boundary is found when a perfect superposition between the ground and target state is reached.

In this work we considered the specific case of an exciton state of a four-atom chain. In that case, when investigating two-atom entanglement the permutation of the k' -entangled state is rendered unnecessary since $k' = k = 2$. Unfortunately, this is no longer true for $k = 3$, where we did have to account for all permutations.

References

1. Lukin, M. Colloquium: Trapping and manipulating photon states in atomic ensembles. *Rev. Mod. Phys.* **75**, 457 (2003).
2. Lukin, M. *et al.* Dipole blockade and quantum information processing in mesoscopic atomic ensembles. *Phys. Rev. Lett.* **87**, 037901 (2001).
3. Hammerer, K., Sørensen, A. & Polzik, E. Quantum interface between light and atomic ensembles. *Rev. Mod. Phys.* **82**, 1041 (2010).
4. Wineland, D., Bollinger, J., Itano, W., Moore, F. & Heinzen, D. Spin squeezing and reduced quantum noise in spectroscopy. *Phys. Rev. A* **46**, R6797 (1992).
5. Sangouard, N., Simon, C., De Riedmatten, H. & Gisin, N. Quantum repeaters based on atomic ensembles and linear optics. *Rev. Mod. Phys.* **83**, 33 (2011).
6. Leroux, I., Schleier-Smith, M. & Vuletić, V. Focus: Atomic clock beats the quantum limit. *Phys. Rev. Focus* **25**, 24 (2010).
7. Davies, E. *Quantum theory of open systems* (Academic Press, 1976).
8. Gardiner, C. & Zoller, P. *Quantum noise: a handbook of Markovian and non-Markovian quantum stochastic methods with applications to quantum optics*, vol. 56 (Springer Science & Business Media, 2004).
9. Gheri, K., Alge, W. & Grangier, P. Quantum analysis of the photonic blockade mechanism. *Phys. Rev. A* **60**, R2673 (1999).
10. Zoubi, H. & Ritsch, H. Metastability and directional emission characteristics of excitons in 1D optical lattices. *EPL* **90**, 23001 (2010).
11. Lehmberg, R. Radiation from an N-atom system. I. General formalism. *Phys. Rev. A* **2**, 883 (1970).
12. Freedhoff, H. Collective atomic effects in resonance fluorescence: Dipole-dipole interaction. *Phys. Rev. A* **19**, 1132 (1979).
13. Zhu, B., Schachenmayer, J., Xu, M., Herrera, F., Restrepo, J., Holland, M. & Rey, A. Synchronization of interacting quantum dipoles. *New Journal of Physics* **17**, 083063 (2015).
14. Zoubi, H. & Ritsch, H. Bright and dark excitons in an atom-pair-filled optical lattice within a cavity. *EPL* **82**, 14001 (2008).
15. Ostermann, L., Ritsch, H. & Genes, C. Protected state enhanced quantum metrology. *Phys. Rev. Lett.* **111**, 123601 (2013).
16. Ostermann, L., Plankensteiner, D., Ritsch, H. & Genes, C. Protected subspace Ramsey spectroscopy. *Phys. Rev. A* **90**, 053823 (2014).
17. Zoubi, H. & Ritsch, H. Optical properties of collective excitations for an atomic chain with vacancies. *EPL D* **66**, 292 (2012).
18. Böttcher, A. & Silbermann, B. *Introduction to large truncated Toeplitz matrices* (Springer Science & Business Media, 2012).

19. Dicke, R. Coherence in spontaneous radiation processes. *Phys. Rev.* **93**, 99 (1954).
20. Zoubi, H. & Ritsch, H. Excitons and cavity optical lattice ultracold atoms. *Advances in Atomic, Molecular, and Optical Physics* **62**, 171 (2013).
21. Bloom, B. *et al.* An optical lattice clock with accuracy and stability at the 10^{-18} level. *Nature* **506**, 71–75 (2014).
22. Ushijima, I., Takamoto, M., Das, M., Ohkubo, T. & Katori, H. Cryogenic optical lattice clocks. *Nature Photonics* **9**, 185 (2015).
23. Maier, T., Krämer, S., Ostermann, L. & Ritsch, H. A superradiant clock laser on a magic wavelength optical lattice. *Optics Express* **22**, 13269–13279 (2014).
24. Sørensen, A. & Mølmer, K. Entanglement and extreme spin squeezing. *Phys. Rev. Lett.* **86**, 4431 (2001).
25. Haas, F., Volz, J. *et al.* Entangled states of more than 40 atoms in an optical fiber cavity. *Science* **344**, 180 (2014).
26. McConnell, R., Zhang, H. *et al.* Entanglement with negative Wigner function of almost 3,000 atoms heralded by one photon. *Nature* **519**, 439 (2015).
27. Olmos, B. *et al.* Long-range interacting many-body systems with alkaline-earth-metal atoms. *Physical review letters* **110**, 143602 (2013).
28. Ueberholz, B., Kuhr, S., Frese, D., Gomer, V. & Meschede, D. Cold collisions in a high-gradient magneto-optical trap. *Journal of Physics B: Atomic, Molecular and Optical Physics* **35**, 4899 (2002).
29. Yoon, S. *et al.* Characteristics of single-atom trapping in a magneto-optical trap with a high magnetic-field gradient. *Journal of Physics: Conference Series* **80**, 012046 (2007).
30. Yan, B. *et al.* Observation of dipolar spin-exchange interactions with lattice-confined polar molecules. *Nature* **501**, 521–525 (2013).
31. Neumann, P. *et al.* Quantum register based on coupled electron spins in a room-temperature solid. *Nature Physics* **6**, 249–253 (2010).
32. Zoubi, H. & Ritsch, H. Hybrid quantum system of a nanofiber mode coupled to two chains of optically trapped atoms. *New Journal of Physics* **12**, 103014 (2010).
33. Meiser, D. & Holland, M. Steady-state superradiance with alkaline-earth-metal atoms. *Phys. Rev. A* **81**, 033847 (2010).
34. Sandner, K. *et al.* Strong magnetic coupling of an inhomogeneous nitrogen-vacancy ensemble to a cavity. *Phys. Rev. A* **85**, 053806 (2010).
35. Lalumière, K. *et al.* Input-output theory for waveguide QED with an ensemble of inhomogeneous atoms. *Phys. Rev. A* **88**, 043806 (2013).
36. Johansson, J., Nation, P. & Nori, F. Qutip 2: A Python framework for the dynamics of open quantum systems. *Comput. Phys. Commun.* **184**, 1234 (2013).

Acknowledgements

We acknowledge financial support from the SFB through the FoQus project (D. P.), DARPA through the QUASAR project (L. O. and H. R.) and from the Austrian Science Fund (FWF) via project P24968-N27 (C. G.). Furthermore, we acknowledge the use of the QuTip open-source software.³⁶ H.R. thanks Vladan Vuletic for helpful discussions. C. G. thanks M. W. Mitchell for the suggestion of energetic addressing of collective states.

Author contributions statement

C. G. conceived the ideas and supervised the work. D. P. developed the concepts, conducted analytical calculations, took the main role in writing the manuscript and wrote numerical simulations, with support from L. O. especially in generalizing the depth of entanglement. H. R. provided guidance and expertise. The manuscript has been reviewed and edited by all authors.

Additional information

No competing financial interests arise in the funding of this work.